



Spring 2021

Structure of Blood Coagulation Factor VIII in Complex with Anti-C2 Domain Inhibitory Antibody

Estelle K. Ronayne
Western Washington University

Shaun C. Peters
Western Washington University


Joseph Gish
Western Washington University

Celena Wilson
Western Washington University

H Trent Spencer
Emory University

See next page for additional authors

Follow this and additional works at: https://cedar.wwu.edu/wwu_honors

 Part of the [Art and Design Commons](#), [Biochemistry, Biophysics, and Structural Biology Commons](#), and the [Chemistry Commons](#)

Recommended Citation

Ronayne, Estelle K.; Peters, Shaun C.; Gish, Joseph; Wilson, Celena; Spencer, H Trent; Doering, Christopher B.; Lollar, Pete; Spiegel, P Clint Jr.; and Childers, Kenneth C., "Structure of Blood Coagulation Factor VIII in Complex with Anti-C2 Domain Inhibitory Antibody" (2021). *WWU Honors Program Senior Projects*. 487. https://cedar.wwu.edu/wwu_honors/487

This Project is brought to you for free and open access by the WWU Graduate and Undergraduate Scholarship at Western CEDAR. It has been accepted for inclusion in WWU Honors Program Senior Projects by an authorized administrator of Western CEDAR. For more information, please contact westerncedar@wwu.edu.

Authors

Estelle K. Ronayne, Shaun C. Peters, Joseph Gish, Celena Wilson, H Trent Spencer, Christopher B. Doering, Pete Lollar, P Clint Spiegel Jr., and Kenneth C. Childers

Structure of Blood Coagulation Factor VIII in Complex with Anti-C2 Domain Inhibitory Antibody

Estelle K. Ronayne¹, Shaun C. Peters¹, Joseph Gish¹, Celena Wilson¹, H. Trent Spencer², Christopher B. Doering², Pete Lollar², P. Clint Spiegel, Jr.¹, Kenneth C. Childers¹.

¹Department of Chemistry, Western Washington University, Bellingham, WA, USA

²Department of Pediatrics, Aflac Cancer and Blood Disorders Center, Children's Healthcare of Atlanta, Emory University, Atlanta, GA, USA

Abstract

Factor VIII (fVIII) is a procoagulant protein that binds to activated factor IX (fIXa) on platelet surfaces to form the intrinsic tenase complex. Due to the high immunogenicity of fVIII, generation of antibody inhibitors is a common occurrence in patients during hemophilia A treatment and spontaneously occurs in acquired hemophilia A patients. Non-classical antibody inhibitors, which block fVIII activation by thrombin and formation of the tenase complex, are the most common anti-C2 domain pathogenic inhibitors in hemophilia A murine models and have been identified in patient plasmas. In this study, we report on the X-ray crystal structure of a B domain-deleted bioengineered fVIII bound to the non-classical antibody inhibitor, G99. While binding to G99 does not disrupt the overall domain architecture of fVIII, the C2 domain undergoes an ~ 8 Å translocation that is concomitant with breaking multiple domain-domain interactions. Analysis of normalized B-factor values revealed several solvent-exposed loops in the C1 and C2 domains which experience a decrease in thermal motion in the presence of inhibitory antibodies. Our results enhance our understanding on the structural nature of binding non-classical inhibitors and provide a structural dynamics-based rationale for cooperativity between anti-C domain inhibitors.

Introduction

Hemophilia A is an X-linked recessive disorder caused by mutation to the *F8* gene which results in a deficiency of coagulation factor VIII (fVIII), where severe mutations abolish fVIII production completely. Patients with hemophilia A are prone to uncontrolled bleeding events and require regular infusions of recombinant or plasma-derived fVIII to maintain functional coagulation (1,2). In approximately 30% of hemophilia A treatment cases, patients will produce antibodies that inhibit infused fVIII and reduce treatment efficacy (3,4). Furthermore, acquired hemophilia A can develop in healthy individuals through an autoimmune response, producing antibody inhibitors which bind to and inhibit the cofactor activity of native fVIII (5). Immune tolerance induction has been demonstrated to overwhelm the immune system through frequent, high-dosages of fVIII with modest success (3), but can be a physical and financial burden for the patient (6).

Coagulation fVIII is a multidomain glycoprotein that circulates in the bloodstream as a heterodimer of the heavy chain (A1-A2) and light chain (A3-C1-C2) while bound to von Willebrand factor (vWf) to

prevent premature clearance and/or degradation (2,7). Once cleaved by thrombin, activated fVIII (fVIIIa) dissociates from vWf and binds activated platelet surfaces, likely through embedding several solvent-exposed hydrophobic loops on the C1 and C2 domains (8–10). Binding to activated factor IX (fIXa), a serine protease, forms the ‘intrinsic’ tenase complex which amplifies the generation of activated factor X (fXa) and subsequently thrombin.

One example of a fVIII replacement therapeutic is ET3i, a bioengineered human-porcine chimera of B-domain deleted fVIII. ET3i consists of porcine A1 and A3 domains and human A2, C1, and C2 domains. Domain swapping was employed to increase protein expression and stability, while still maintaining function (11,12). Additionally, ET3i undergoes slower A2 dissociation upon activation by thrombin, prolonging half-life (13).

Previous studies indicate the A2, C1, and C2 domains to be highly immunogenic, where C2 is immunodominant (4,14–17). Anti-C2 domain inhibitors represent a diverse group of fVIII neutralizing antibodies and are categorized as classical and non-classical antibodies (18–20). Classical antibodies inhibit fVIII binding to vWf and platelet surfaces and their associated epitopes are categorized into groups A, AB or B (18). X-ray crystal structures of the isolated C2 domain bound classical inhibitors such as BO2C11 (21) and 3E6 (22,23) have identified unique conformational epitopes and demonstrated how inhibitor binding reduces circulatory levels of fVIII. Conversely, non-classical antibodies prevent fVIII activation by thrombin or fXa and their epitopes are categorized into groups BC and C (18). Non-classical antibodies are the most common pathogenic inhibitors in hemophilia A murine models (18) and inhibitors with overlapping epitopes have been detected in hemophilia A patient plasma (19). Group BC inhibitors are the most common anti-C2 antibodies and display above-average titer levels, particularly in patients with acquired hemophilia A (18), representing a significant clinical complication. In the presence of non-classical inhibitors, the binding of classical inhibitors to fVIII has been shown to increase (24). Additionally, hydrogen-deuterium exchange (HDX) protection patterns suggest cooperativity between anti-fVIII inhibitors, G99 and 3E6 (25).

The pathogenic, non-classical antibody inhibitor G99 is a group BC inhibitor and binds to several solvent-exposed loops in the C2 domain that are predicted to interact with thrombin and fIXa (26,27). Epitope mapping based on HDX rates indicate residues 2200–2228 are a major determinant in G99 binding (28), including K2227 which, upon substitution with glutamic acid, abrogates fVIII binding to G99 (18). The crystal structure of the isolated C2 domain bound to G99 identified a conformational epitope composed of multiple loops and revealed K2227 forms multiple electrostatic contacts with the G99 light chain (22). Here, we present the crystal structure of ET3i (29–31) bound to the G99 antigen binding fragment (F_{AB}). Our structure represents the first crystal structure of a fVIII replacement therapeutic bound to an anti-C2 inhibitor, providing insight into how non-classical inhibitors alter the C2 domain conformation of mature fVIII and allosterically influence the thermal motion of nearby epitopes.

Materials and Methods

Expression and Purification of ET3i

ET3i was expressed and purified as previously described (29,30) to a final concentration of 0.8 mg/mL and stored in 50 mM HEPES, pH 7.4, 5 mM CaCl₂ and 350 mM NaCl at -80 °C.

Purification of G99 F_{AB} Fragments

G99 monoclonal antibodies were expressed and purified in hybridoma cell lines and F_{AB} fragments were prepared as previously described (18,22). Briefly, large-scale antibody production was performed at the Antibody Production Facility at the Fred Hutch (Seattle, WA). Immunoglobulin (IgG) and F_{AB} purifications were completed with Protein A Plus spin columns and immobilized papain kits (Thermo Scientific, Rockford, IL) according to the manufacturer's protocols. Purified F_{AB} fragments were stored at a final concentration of 10 mg/mL at -80 °C in F_{AB} storage buffer (25 mM Tris-HCl pH 7.2, 100 mM NaCl).

Crystallization, Data Collection, and Refinement

The ET3i:G99 F_{AB} complex was formed at a 1:1.2 stoichiometric ratio in 50 mM Tris HCl (pH 7.4), 200 mM NaCl, and 2.5 mM CaCl₂ and purified using a 100 kDa MWCO spin column (Amicon) to 1 mg/mL. Initial crystal conditions were determined via high-throughput microbatch crystallization using the Hauptman-Woodward High-Throughput Crystallization Center (Buffalo, NY) (27). Diffraction quality crystals were subsequently grown by hanging drop vapor diffusion in a 1:1 (v/v) ratio of the ET3i:G99 protein complex and crystallization solution containing 50 mM malic acid (pH 7.0) and 8-18% (w/v) PEG 1500, PEG 6000, or PEG 10,000. Crystals were cryoprotected in mother liquor with the stepwise addition of 30% (v/v) glycerol. X-ray diffraction data were collected on the Advanced Light Source (ALS) Berkeley Center for Structural Biology (BCSB) beamline 5.0.1 (Berkeley, CA). Data collection and processing were performed with Adxv, XDS and CCP4 (32). Phasing of the ET3i:G99 crystals was determined with PHASER-MR using a fragment-based molecular replacement approach with the previously determined 3.2 Å structure of ET3i (PDB ID: 6MF0) and the 2.47 Å structure of human factor VIII C2 domain in complex with murine inhibitory antibodies 3E6 and G99 (PDB ID: 4KI5) (22,31,33). Model building and refinement were performed with WinCoot and PHENIX, respectively (34). All figures were generated with the PyMOL Molecular Graphics System, Version 2.0 (Schrödinger, LLC).

Results

Crystal Structure of Factor VIII in Complex with the Anti-C2 Domain G99 Antibody

The X-ray crystal structure of the ET3i B domain-deleted fVIII construct bound to G99 was determined at 4.15 Å resolution and refined to R_{work}/R_{free} values of 0.2998/0.3384 (PDB ID: 7KBT) (Figure 1A, Table S1). The asymmetric unit (ASU) contains one molecule consisting of the A1, A2, A3, C1, and C2 domains of ET3i and the variable domains of the heavy and light chains of G99. While the F_{AB} constant domains were included in the protein complex, these domains could not be modeled into the final structure, presumably due to flexibility, and thus were excluded. The ET3i:G99 complex superimposes well with the crystal structure of the isolated C2 domain bound to G99 (PDB ID: 4KI5) (22) with a root-mean-square deviation (RMSD) value of 0.81 Å² (Figure 1B). Both complexes have structurally identical epitopes for the G99 inhibitor antibody which encompass residues 2193-2194, 2222-2229, 2161-2163, 2269-2282, and 2307-2311 (Figure 1C). The nature of the C2/G99 binding interface relies on a combination of polar and hydrophobic interactions. Figure 1D illustrates how K2227 is a critical residue for binding to G99, participating in multiple electrostatic interactions with E50, T99, and Y96. The epitope spanning residues 2222-2229 provides multiple points of contact with the heavy chain of G99 (Figure 1E), including E2228 which has been proposed to interact with the GlA domain of fIXa (27). Lastly, residues L2261, L2273,

V2280, and V2282, previously suggested as a binding site for thrombin (26), form direct, extensive contacts with the G99 light chain (Figure 1F). Our structure of ET3i bound to the G99 F_{AB} fragment illustrates how non-classical inhibitors potentially block the binding of thrombin, fXa and fIXa, thus preventing dissociation from vWf and formation of the tenase complex.

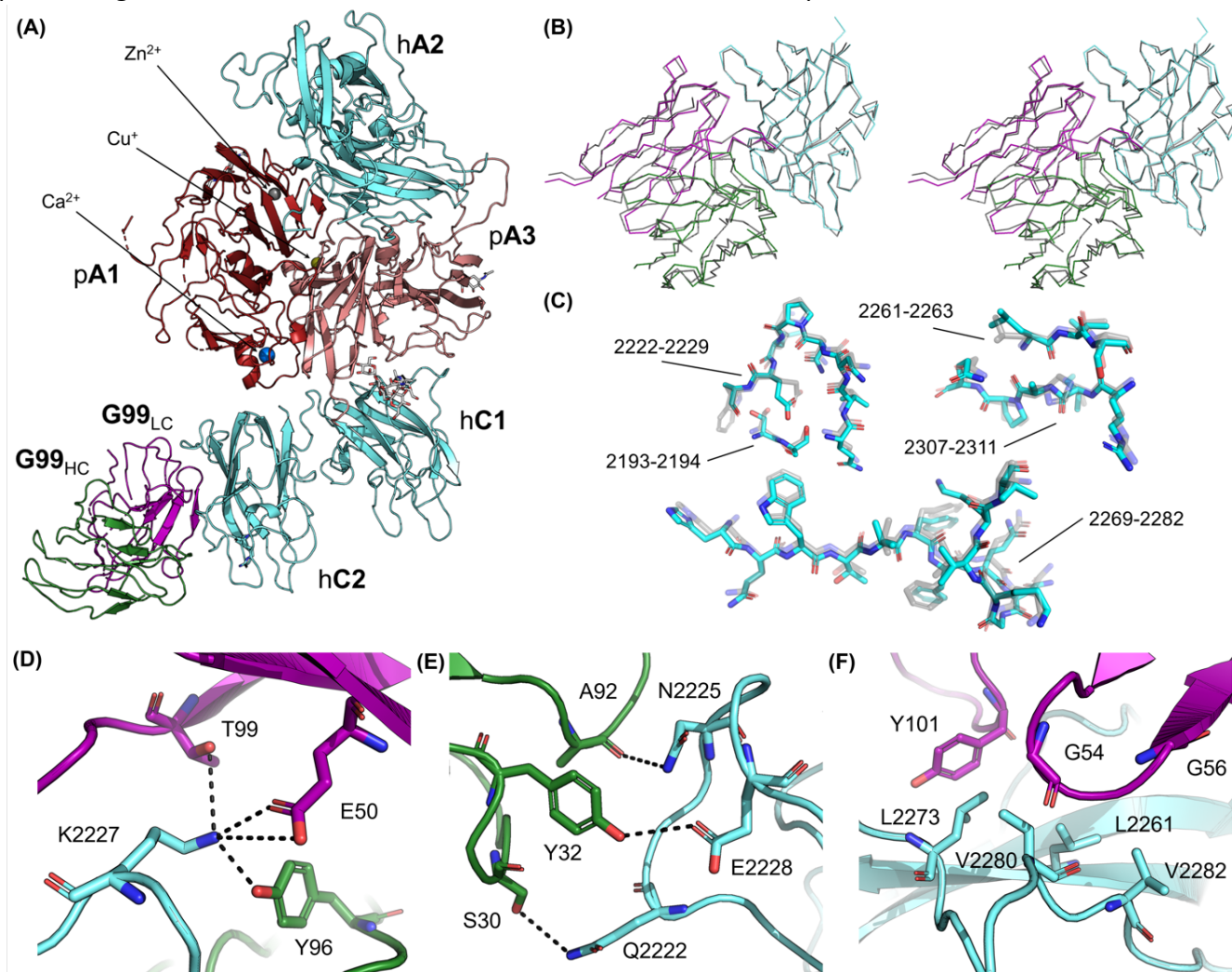


Figure 1. Crystal structure of ET3i bound to the G99 F_{AB} fragment. (A) Cartoon representation of the B domain deleted bioengineered fVIII construct (ET3i) bound to the variable domain of G99 inhibitor antibody. Porcine A1 and A3 (pA1 and pA3) domains are colored dark red and pink, respectively, and human A2, C1, and C2 (hA2, hC1, and hC2) domains are colored cyan. Heavy and light chains of the G99 F_{AB} fragment (G99_{HC} and G99_{LC}) are colored green and purple, respectively. N-acetylglucosamine modifications are depicted as sticks. (B) Ribbon diagram of aligned C2 domain (cyan) and G99 heavy and light chains (green and purple, respectively) from the ET3i:G99 crystal structure and of the isolated C2 domain bound to G99 (grey; PDB ID: 4KI5) in stereo view. (C) Stick representation of the G99 epitope from the ET3i:G99 (cyan) and C2:G99 (grey, faded) crystal structures. (D,E) Electrostatic contacts between ET3i epitope 2222-2229 (cyan) and G99 heavy chain (green) and light chain (purple). Dotted lines depict hydrogen bonds (distance ≤ 5 Å). (F) Hydrophobic residues along the ET3i epitope 2269-2282 (cyan) buried by the G99 light chain (purple).

Binding G99 Induces a Conformational Rearrangement to the C2 Domain in Mature Factor VIII

Alignment of the ET3i:G99 complex to the unbound ET3i structure (PDB ID: 6MF0) (31) suggests that binding G99 does not disrupt the overall ET3i structure, with an average RMSD of 0.68 Å² (Figure 2A).

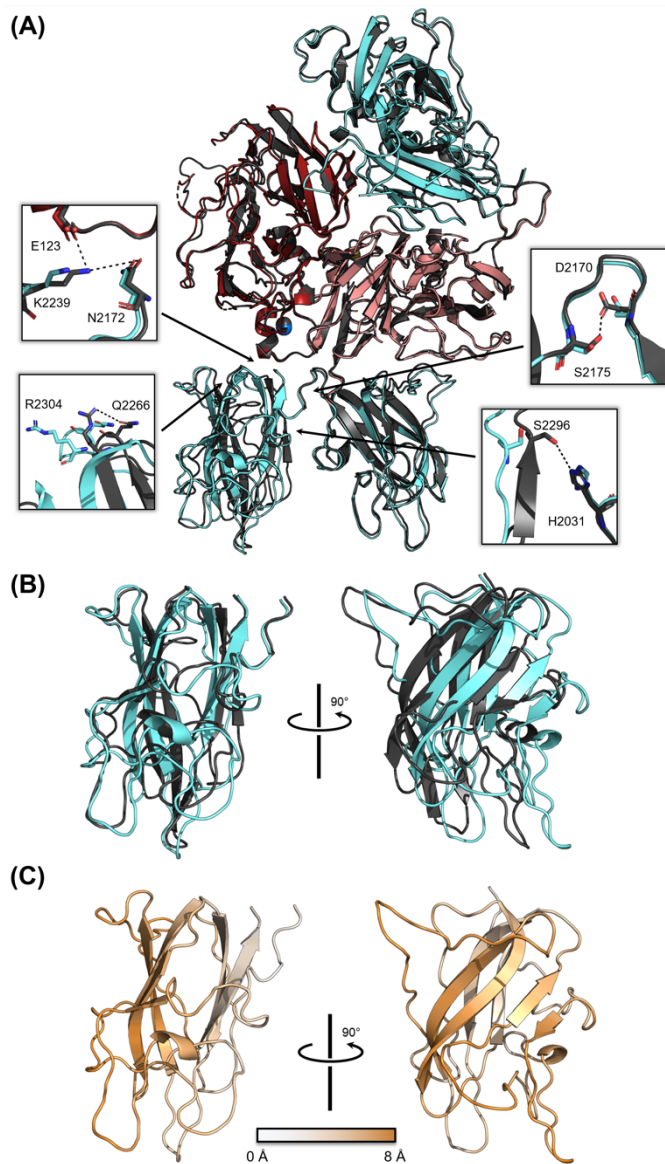


Figure 2. Structural alignment of unbound ET3i and ET3i:G99 crystal structures. (A) Alignment of unbound ET3i (grey) and ET3i:G99 (A1: dark red, A3: pink, A2/C1/C2: cyan). Insets depict intramolecular contacts that are broken in the ET3i:G99 structure. (B) Alignment of the C2 domain from unbound ET3i structure (grey) and ET3i:G99 structure (cyan). (C) Structure of the C2 domain from the ET3i:G99 complex colored as a function of RMSD from alignment with unbound ET3i. White: low RMSD shifts, orange: large RMSD shifts.

structure thermostability, with low values indicating rigidity and high values indicating flexibility (units, Å²). In addition to the unbound ET3i and ET3i:G99 crystal structures, we also included the crystal structure of ET3i complexed with the anti-C1 domain inhibitor 2A9 (PDB ID: 7K66) in our analysis as the C2 domain in this structure undergoes a similar translocation (36). To better compare between each

The C2 domain, however, shows the largest conformational change upon binding G99 (Figures 2B, 2C), undergoing an ~8 Å translocation relative to the other ET3i domains. Most of these conformational changes are localized to several loops proximal to the G99 epitope, including residues 2256-2265, 2270-2285, and 2305-2314. This rearrangement to the C2 domain is concomitant with breaking multiple interfacial contacts with the adjacent A1 and C1 domains (Figure 2A). The A1/C2 interface includes interactions between amino acids E123, N2172, and K2239 that are disrupted due to K2239 shifting by 5 Å in the ET3i:G99 structure. The C1/C2 interface includes interactions between amino acids H2031 and S2296, and D2170 and S2175, both of which become disrupted in the ET3i:G99 complex. Lastly, the ET3i:G99 crystal structure reveals loss of an intramolecular contact within the C2 domain between R2304 and Q2266. While the extent of disruption to these interactions is not definitive given the lower resolution of the crystallographic data, the structure of ET3i:G99 does show significant rearrangement to the C2 domain with the greatest conformational changes occurring to the aforementioned regions.

Analysis of B-Factor Values from Multiple ET3i Crystal Structures

To further investigate how inhibitor binding influences the flexibility of C domain epitopes, we performed a comparative B-factor analysis on the C1 and C2 domains from several crystal structures of ET3i bound to antibody inhibitors as well as the unbound ET3i structure (Figures 3A, 3B). B-factor values are calculated by the spatial fluctuation of atoms in a crystal structure from their equilibrium positions (35) and provide insight into protein

crystal dataset and reduce bias in this study, normalized B-factor values (B') were calculated using the following equation:

$$B' = \frac{B}{(B_{average})(Resolution)} \quad (1)$$

where B is the raw atomic B-factor, $B_{average}$ is the average B-factor of the ET3i molecule in the crystal asymmetric unit, and Resolution is the reported atomic resolution for the respective structure. Model A of the unbound ET3i crystal structure, which has two ET3i molecules in the ASU (31), was used to compare with the antibody-bound structures.

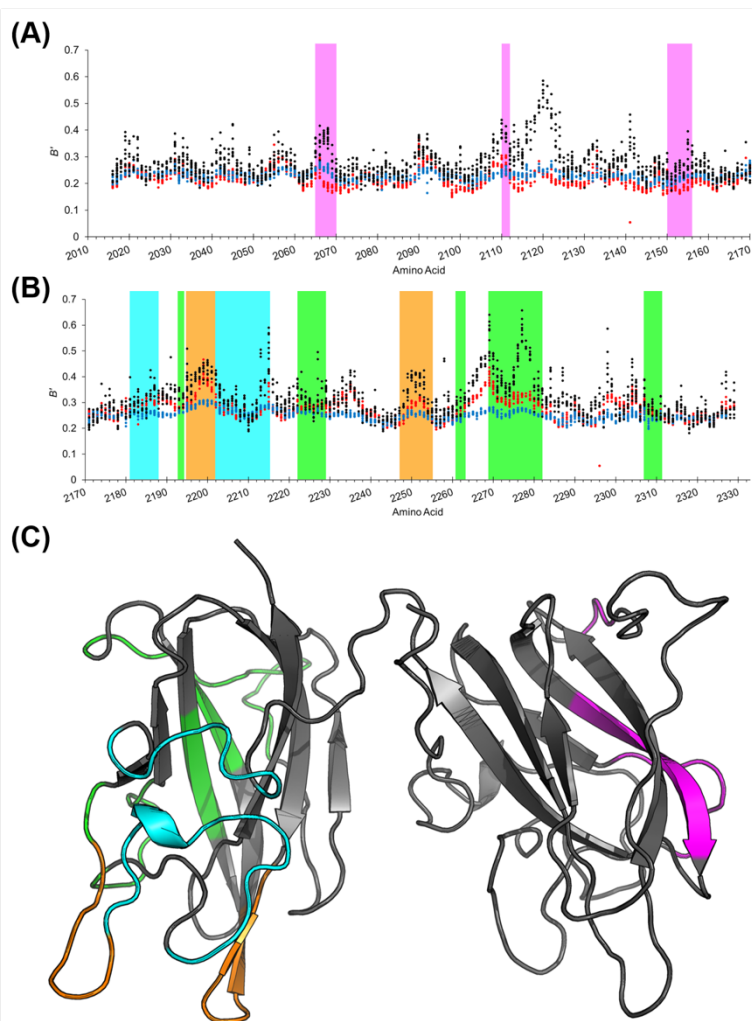


Figure 3. Anti-C domain inhibitors reduce atomic B-factors on solvent-exposed loops. (A,B) Normalized atomic B-factors averaged for each epitope in the (A) C1 domain and (B) C2 domain from unbound ET3i (black, PDB ID: 6MF0), ET3i:G99 (blue, PDB ID: 7KBT), and ET3i:2A9 (red, PDB ID: 7K66). **(C)** Cartoon representation of the C1 and C2 domains from the unbound ET3i crystal structure (PDB ID: 6MF0, model A). Antibody epitopes are highlighted (2A9: magenta, G99: green, 3E6: cyan, BO2C11: orange).

The average B' values at known C1 and C2 domain epitopes (Figure 3C) from three ET3i crystal structures were tabulated for comparison (Table 1). As expected, regions that experience some of the greatest decreases in B' values occur directly at the epitopes from the antibody-bound structures. Residues 2065-2070, 2110-2112, and 2150-2156 in the ET3i:2A9 structure, which encompass the 2A9 epitope, have 35.2%, 27.2%, and 26.1% lower B' values, respectively, compared to the free ET3i structure (Figure S1). Similarly, residues 2269-2282, which form extensive interactions with the G99 antibody, have a 37.9% lower average B' value in the ET3i:G99 complex than the unbound ET3i structure (Figure S2). These observed differences in B' values are due to the inhibitory antibody binding to the respective epitope and reducing atomic motions.

Previous work focusing on the atomic B-factors from crystal structures of the isolated C2 domain bound to classical and non-classical inhibitory antibodies identified fluctuations to the thermostability in certain epitopes (17,23). We sought to expand our understanding on this topic by calculating the B' values in the C1 and C2 domain epitopes when the opposing domain was bound to an inhibitory antibody. Our results indicate that antibody binding is a potent allosteric modulator of

atomic motions to adjacent epitope (Table 1). For instance, residues 2269-2282, which participate in binding G99 to the C2 domain, have a 24.4% lower average B' value in the ET3i:2A9 structure than the unbound ET3i structure. Similarly, B' values from residues that comprise the 2A9 epitope in the ET3i:G99 crystal structure are lower than the unbound ET3i structure, most notably residues 2065-2070 which have a 23.5% lower average B' value. By calculating the average B' value for each amino acid at these epitopes, we determined that P2067 and F2068 of residues 2065-2070 and Q2276, N2277, and G2278 of residues 2069-2282 experience the greatest reduction in atomic motions (Figures S1 and S2). None of the aforementioned “coldspots” participate in lattice contacts within the protein crystal, indicating an alternate mechanism for reducing peptide flexibility. While differences in B' values can be due to variables that are unaccounted for in equation 1, such as crystallization conditions or refinement strategy, these results are indicative of an allosteric relationship between anti-C1 and anti-C2 epitopes in the presence of inhibitor antibodies.

Table 1. Average B' values for C1 and C2 domain epitopes. Values in parentheses depict percent differences from the unbound ET3i structure. Bold values represent differences that are greater than the average ET3i molecule (“coldspots”).

	ET3i	ET3i:G99	ET3i:2A9
A1-A2/A3-C1-C2	0.307	0.241 (-21.5%)	0.255 (-16.9%)
2A9 epitope			
2065-2070	0.322	0.247 (-23.5%)	0.209 (-35.2%)
2110-2112	0.352	0.235 (-33.1%)	0.256 (-27.2%)
2150-2156	0.260	0.218 (-16.4%)	0.192 (-26.1%)
G99 epitope			
2193-2194	0.319	0.264 (-17.5%)	0.279 (-12.6%)
2222-2229	0.323	0.263 (-18.4%)	0.284 (-12.0%)
2261-2263	0.294	0.241 (-18.0%)	0.260 (-11.5%)
2269-2282	0.422	0.262 (-37.9%)	0.319 (-24.4%)
2307-2311	0.286	0.239 (-16.3%)	0.266 (-7.1%)
3E6 epitope			
2181-2188	0.311	0.257 (-17.4%)	0.293 (-5.9%)
2202-2215	0.326	0.269 (-17.5%)	0.267 (-18.3%)
BO2C11 epitope			
2195-2202	0.404	0.291 (-28.0%)	0.339 (-16.0%)
2247-2255	0.337	0.251 (-25.5%)	0.270 (-19.9%)

We next investigated the atomic thermostability for residues spanning the epitopes for 3E6 and BO2C11 antibodies, which bind to unique regions on the C2 domain (Figure 3C) and are categorized as classical inhibitors (21–23), in the ET3i:G99 and ET3i:2A9 crystal structures. We measured reduced B' values for the 3E6 epitope in the ET3i:2A9 and ET3i:G99 structures when compared with the unbound ET3i structure. Specifically, the 3E6 epitope spanning residues 2202-2215 had an 18% lower average B' in

both inhibitor-bound crystal structures (Table 1, Figure S3). Residues 2195-2202 and 2247-2255, which encompass the BO2C11 epitope (21), have 16% and 19.9% lower B' values in the ET3i:2A9 crystal structure, respectively, and are even lower in the ET3i:G99 structure (28.0% and 25.5%, respectively) (Table 1, Figure S4). Taken together, these results support the hypothesis that these regions on the C2 domain become more rigid when bound to either G99 or 2A9.

Discussion

In this study, we report on the crystal structure of ET3i, a bioengineered fVIII molecule, bound to the pathogenic, non-classical antibody inhibitor G99. While the A domains are structurally unperturbed by G99 binding, the C2 domain undergoes an ~ 8 Å translocation and loses multiple intramolecular contacts with the adjacent A1 and C1 domains. Mutations at the A1/C2 and C1/C2 domain interfaces have been identified in multiple hemophilia A cases, including E123K, K2239E, and R2304L/G/C (37–40). Considering the crystal structure of ET3i:G99 indicates binding to G99 disrupts these domain-domain contacts, we speculate how mutations to these regions influence the C2 domain conformation and inhibitor binding. In a previous surface plasmon resonance-based study with a suite of fVIII point mutants, researchers mapped the epitopes of 11 anti-C2 antibody inhibitors and identified several residues that are not part of a contiguous epitope, yet significantly impact binding to anti-C2 inhibitors when mutated (41). K2239, which participates in multiple hydrogen bonds at the A1/C2 domain interface (Figure 2A), demonstrated slightly stronger binding with the classical antibody 3E6 when substituted with alanine. Furthermore, R2304C, which is linked to moderate cases of hemophilia A and high inhibitor titer levels (38,40), has been proposed to destabilize fVIII without disrupting vWf and phospholipid binding (42). These data are indicative of a unique relationship between C2 domain-domain contacts and fVIII immunogenicity. Disruption to domain interfacial contacts may induce a structural rearrangement to the C2 domain and enhance immune recognition and inhibitor binding. Our structure of the ET3i:G99 complex provides evidence for a connection between disruption to domain-domain contacts near the C2 domain and inhibitor binding.

Normalization and comparison of B-factors between different crystal structures has previously been utilized to study the effects of ligand binding (43), mutagenesis (44), environmental pH (45), as well as protein engineering to enhance stability (46). Our analysis of normalized B-factors from several ET3i structures in the absence and presence of inhibitor antibodies suggests that binding G99 induces structural rigidity in multiple solvent-exposed regions of the C domains that are not a part of the G99 epitope. HDX protection patterns have been identified for residues 2231-2252 using the isolated C2 domain bound to G99 (28). Our results support these findings, with the greatest reduction in atomic motions occurring to residues 2249-2252 at both the amino acid functional group and the peptide backbone (Figure S2).

Adjustments to the thermostability in certain fVIII epitopes raise important questions regarding immune recognition and cooperativity between classical and non-classical anti-C2 domain inhibitors. Indeed, synthetic peptides encompassing the G99 epitope have been shown to stimulate CD4+ T-cell proliferation and induce an immune response, including residues 2301-2320 which had the strongest response among acquired hemophilia A patients (17). Because the degree of peptide flexibility is a strong determinant in T-cell recognition and binding to T-cell receptors (47–49), reducing the dynamic mobility

in certain fVIII epitopes is a potential mechanism in fVIII immune recognition. Furthermore, group A classical inhibitors have elevated association rates with fVIII when in the presence of non-classical group BC antibodies (24,50), providing evidence for a cooperative immune response to fVIII. HDX measurements on the isolated C2 domain pre-mixed with G99 and 3E6 had stronger protection patterns than the individually bound complexes (25). Structural characterization of the C2 domain bound to G99 and 3E6 FAB fragments supports a polyclonal response to fVIII (22,51). Our analysis of normalized B-factors suggests that cooperativity between inhibitors relies on reducing local disorder to these regions. Lowering atomic motions may reduce the conformational diversity of certain epitopes, thereby decreasing the entropic cost in macromolecular association, to provide a high-affinity binding site for antibody inhibitors (23,52,53). Modification of these epitopes to prevent rigidification and promote conformational diversity may present a novel strategy in the design of fVIII replacement therapeutics with reduced immunogenicity.

Data Availability Statement

Atomic coordinates for the ET3i:G99 crystal structures were deposited in the Protein Data Bank (code 7KBT). The original contributions presented in this study are included in this article and the Supplementary Material. Further inquiries can be directed to the corresponding authors.

Author Contributions

E.K.R. planned experiments, performed experiments, analyzed data, and assisted in writing the manuscript. S.C.P., J.S.G., and C.W. performed experiments and assisted in analyzing data. H.T.S, C.B.D. and P.L. developed expression and purification procedures for ET3i and G99. P.C.S. and K.C.C. planned experiments, analyzed data, and wrote the manuscript.

Funding

The Berkeley Center for Structural Biology is supported in part by the Howard Hughes Medical Institute. The Advanced Light Source is a Department of Energy Office of Science User Facility under Contract No. DE-AC02-05CH11231. The Pilatus detector on 5.0.1. was funded under NIH grant S10OD021832. The ALS-ENABLE beamlines are supported in part by the National Institutes of Health, National Institute of General Medical Sciences, grant P30 GM124169. This work was supported by the Dreyfus Foundation (Henry Dreyfus Teacher-Scholar Award), the National Science Foundation (MRI 1429164) and the National Institutes of Health/National Heart, Lung and Blood Institute (award numbers R15HL103518 and U54HL141981 to PCS, award numbers R44HL117511, R44HL110448, U54HL112309 and U54HL141981 to CBD, HTS and PL).

Conflict of Interest

P.L. is inventor on a patent application describing ET3i and is an inventor on patents owned by Emory University claiming compositions of matter that include modified fVIII proteins with reduced reactivity with anti-fVIII antibodies. C.B.D., P.L. and H.T.S. are cofounders of Expression Therapeutics and own equity in the company. Expression Therapeutics owns the intellectual property associated with ET3i.

The terms of this arrangement have been reviewed and approved by Emory University in accordance with its conflict of interest policies.

References

1. Powell JS. Longer-acting clotting factor concentrates for hemophilia. *J Thromb Haemost.* 2015 Jun;13 Suppl 1:S167-75.
2. Fay PJ. Factor VIII structure and function. *Int J Hematol.* 2006 Feb;83(2):103-8.
3. Schep SJ, Schutgens REG, Fischer K, Boes ML. Review of immune tolerance induction in hemophilia A. *Blood Rev.* 2018 Feb 15;32(4):326-38.
4. Lacroix-Desmazes S, Voorberg J, Lillicrap D, Scott DW, Pratt KP. Tolerating factor VIII: recent progress. *Front Immunol.* 2019;10:2991.
5. Tiede A, Collins P, Knoebl P, Teitel J, Kessler C, Shima M, et al. International recommendations on the diagnosis and treatment of acquired hemophilia A. *Haematologica.* 2020 May 7;105(7):1791-801.
6. Neufeld EJ, Sidonio RF, O'Day K, Runken MC, Meyer K, Spears J. Cost analysis of plasma-derived factor VIII/von Willebrand factor versus recombinant factor VIII for treatment of previously untreated patients with severe hemophilia A in the United States. *J Med Econ.* 2018 Aug;21(8):762-9.
7. Hartholt RB, van Velzen AS, Peyron I, Ten Brinke A, Fijnvandraat K, Voorberg J. To serve and protect: The modulatory role of von Willebrand factor on factor VIII immunogenicity. *Blood Rev.* 2017 Jul 4;31(5):339-47.
8. Gilbert GE, Arena AA. Activation of the factor VIIIa-factor IXa enzyme complex of blood coagulation by membranes containing phosphatidyl-L-serine. *J Biol Chem.* 1996 May 10;271(19):11120-5.
9. Madsen JJ, Ohkubo YZ, Peters GH, Faber JH, Tajkhorshid E, Olsen OH. Membrane interaction of the factor viii discoidin domains in atomistic detail. *Biochemistry.* 2015 Oct 6;54(39):6123-31.
10. Wakabayashi H, Fay PJ. Molecular orientation of factor VIIIa on the phospholipid membrane surface determined by fluorescence resonance energy transfer. *Biochem J.* 2013 Jun 1;452(2):293-301.
11. Doering CB, Healey JF, Parker ET, Barrow RT, Lollar P. Identification of porcine coagulation factor VIII domains responsible for high level expression via enhanced secretion. *J Biol Chem.* 2004 Feb 20;279(8):6546-52.
12. Brown HC, Wright JF, Zhou S, Lytle AM, Shields JE, Spencer HT, et al. Bioengineered coagulation factor VIII enables long-term correction of murine hemophilia A following liver-directed adeno-associated viral vector delivery. *Mol Ther Methods Clin Dev.* 2014 Aug 6;1:14036.
13. Lü J, Pipe SW, Miao H, Jacquemin M, Gilbert GE. A membrane-interactive surface on the factor VIII C1 domain cooperates with the C2 domain for cofactor function. *Blood.* 2011 Mar 17;117(11):3181-9.
14. Markovitz RC, Healey JF, Parker ET, Meeks SL, Lollar P. The diversity of the immune response to the A2 domain of human factor VIII. *Blood.* 2013 Apr 4;121(14):2785-95.
15. Kahle J, Orłowski A, Stichel D, Healey JF, Parker ET, Jacquemin M, et al. Frequency and epitope specificity of anti-factor VIII C1 domain antibodies in acquired and congenital hemophilia A. *Blood.* 2017 Aug 10;130(6):808-16.

16. Jones TD, Phillips WJ, Smith BJ, Bamford CA, Nayee PD, Baglin TP, et al. Identification and removal of a promiscuous CD4+ T cell epitope from the C1 domain of factor VIII. *J Thromb Haemost.* 2005 May;3(5):991–1000.
17. Reding MT, Okita DK, Diethelm-Okita BM, Anderson TA, Conti-Fine BM. Human CD4+ T-cell epitope repertoire on the C2 domain of coagulation factor VIII. *J Thromb Haemost.* 2003 Aug;1(8):1777–84.
18. Meeks SL, Healey JF, Parker ET, Barrow RT, Lollar P. Antihuman factor VIII C2 domain antibodies in hemophilia A mice recognize a functionally complex continuous spectrum of epitopes dominated by inhibitors of factor VIII activation. *Blood.* 2007 Dec 15;110(13):4234–42.
19. Meeks SL, Healey JF, Parker ET, Barrow RT, Lollar P. Nonclassical anti-C2 domain antibodies are present in patients with factor VIII inhibitors. *Blood.* 2008 Aug 15;112(4):1151–3.
20. Meeks SL, Healey JF, Parker ET, Barrow RT, Lollar P. Non-classical anti-factor VIII C2 domain antibodies are pathogenic in a murine in vivo bleeding model. *J Thromb Haemost.* 2009 Apr;7(4):658–64.
21. Spiegel PC, Jacquemin M, Saint-Remy JM, Stoddard BL, Pratt KP. Structure of a factor VIII C2 domain-immunoglobulin G4kappa Fab complex: identification of an inhibitory antibody epitope on the surface of factor VIII. *Blood.* 2001 Jul 1;98(1):13–9.
22. Walter JD, Werther RA, Brison CM, Cragerud RK, Healey JF, Meeks SL, et al. Structure of the factor VIII C2 domain in a ternary complex with 2 inhibitor antibodies reveals classical and nonclassical epitopes. *Blood.* 2013 Dec 19;122(26):4270–8.
23. Wuerth ME, Cragerud RK, Spiegel PC. Structure of the Human Factor VIII C2 Domain in Complex with the 3E6 Inhibitory Antibody. *Sci Rep.* 2015 Nov 24;5:17216.
24. Antun AG, Meeks SL, Healey JF, Parker ET, Lollar P. Cooperative Interaction Between Classical and Non-Classical Factor VIII C2 Domain Antibody Epitopes. *Blood.* 2009 Nov 20;114(22):219–219.
25. Meeks SL, Sevy AM, Healey JF, Deng W, Spiegel PC, Li R. Cooperative Binding Of Anti-Factor VIII Inhibitors and Induced Conformational Change Detected By Hydrogen-Deuterium Exchange Mass Spectrometry. *Blood.* 2013 Nov 15;122(21):1088–1088.
26. Nogami K, Shima M, Hosokawa K, Nagata M, Koide T, Saenko EL, et al. Factor VIII C2 domain contains the thrombin-binding site responsible for thrombin-catalyzed cleavage at Arg1689. *J Biol Chem.* 2000 Aug 18;275(33):25774–80.
27. Soeda T, Nogami K, Nishiya K, Takeyama M, Ogiwara K, Sakata Y, et al. The factor VIIIa C2 domain (residues 2228-2240) interacts with the factor IXa Gla domain in the factor Xase complex. *J Biol Chem.* 2009 Feb 6;284(6):3379–88.
28. Sevy AM, Healey JF, Deng W, Spiegel PC, Meeks SL, Li R. Epitope mapping of inhibitory antibodies targeting the C2 domain of coagulation factor VIII by hydrogen-deuterium exchange mass spectrometry. *J Thromb Haemost.* 2013 Dec;11(12):2128–36.
29. Spencer HT, Denning G, Gautney RE, Dropulic B, Roy AJ, Baranyi L, et al. Lentiviral vector platform for production of bioengineered recombinant coagulation factor VIII. *Mol Ther.* 2011 Feb;19(2):302–9.
30. Doering CB, Denning G, Shields JE, Fine EJ, Parker ET, Srivastava A, et al. Preclinical development of a hematopoietic stem and progenitor cell bioengineered factor VIII lentiviral vector gene therapy for hemophilia A. *Hum Gene Ther.* 2018;29(10):1183–201.
31. Smith IW, d'Aquino AE, Coyle CW, Fedanov A, Parker ET, Denning G, et al. The 3.2 Å structure of a bioengineered variant of blood coagulation factor VIII indicates two conformations of the C2

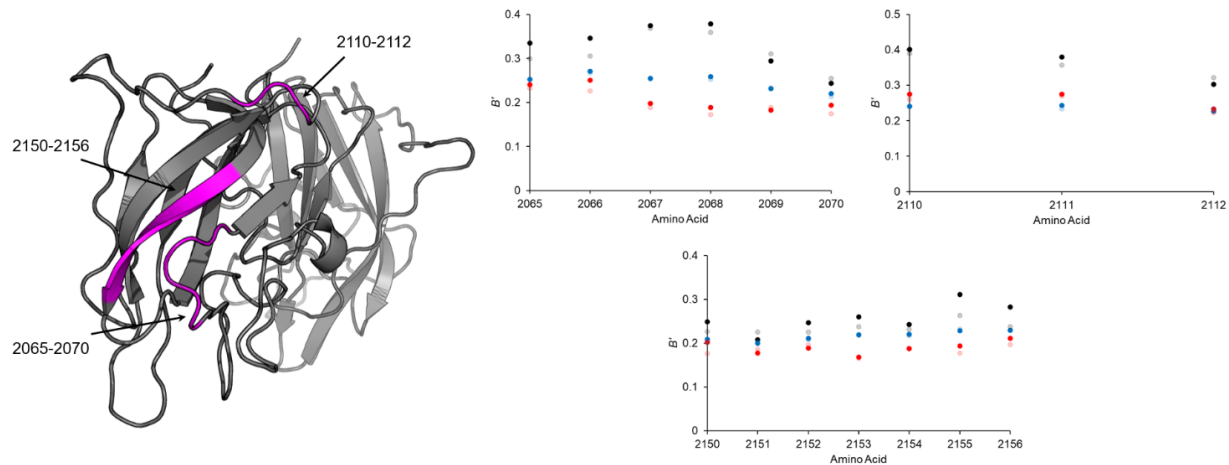
- domain. *J Thromb Haemost.* 2020;18(1):57–69.
32. Winn MD, Ballard CC, Cowtan KD, Dodson EJ, Emsley P, Evans PR, et al. Overview of the CCP4 suite and current developments. *Acta Crystallogr Sect D, Biol Crystallogr.* 2011 Apr;67(Pt 4):235–42.
 33. McCoy AJ, Grosse-Kunstleve RW, Adams PD, Winn MD, Storoni LC, Read RJ. Phaser crystallographic software. *J Appl Crystallogr.* 2007 Aug 1;40(Pt 4):658–74.
 34. Adams PD, Grosse-Kunstleve RW, Hung LW, Ioerger TR, McCoy AJ, Moriarty NW, et al. PHENIX: building new software for automated crystallographic structure determination. *Acta Crystallogr Sect D, Biol Crystallogr.* 2002 Nov;58(Pt 11):1948–54.
 35. Carugo O. Maximal B-factors in protein crystal structures. *Z Kristallogr Cryst Mater.* 2019 Jan 28;234(1):73–7.
 36. Gish JS, Jarvis L, Childers KC, Peters SC, Garrels CS, Smith I, et al. Structure of Blood Coagulation Factor VIII in Complex with an Anti-C1 Domain Pathogenic Antibody Inhibitor. *Blood.* 2021 Feb 2;
 37. Guo Z, Yang L, Qin X, Liu X, Zhang Y. Spectrum of molecular defects in 216 chinese families with hemophilia A: identification of noninversion mutation hot spots and 42 novel mutations. *Clin Appl Thromb Hemost.* 2018 Jan;24(1):70–8.
 38. Miller CH, Benson J, Ellingsen D, Driggers J, Payne A, Kelly FM, et al. F8 and F9 mutations in US haemophilia patients: correlation with history of inhibitor and race/ethnicity. *Haemophilia.* 2012 May;18(3):375–82.
 39. Timur AA, Gürgey A, Aktuglu G, Kavakli K, Canatan D, Olek K, et al. Molecular pathology of haemophilia A in Turkish patients: identification of 36 independent mutations. *Haemophilia.* 2001 Sep;7(5):475–81.
 40. Liu ML, Shen BW, Nakaya S, Pratt KP, Fujikawa K, Davie EW, et al. Hemophilic factor VIII C1- and C2-domain missense mutations and their modeling to the 1.5-angstrom human C2-domain crystal structure. *Blood.* 2000 Aug 1;96(3):979–87.
 41. Nguyen P-CT, Lewis KB, Ettinger RA, Schuman JT, Lin JC, Healey JF, et al. High-resolution mapping of epitopes on the C2 domain of factor VIII by analysis of point mutants using surface plasmon resonance. *Blood.* 2014 Apr 24;123(17):2732–9.
 42. Spiegel PC, Murphy P, Stoddard BL. Surface-exposed hemophilic mutations across the factor VIII C2 domain have variable effects on stability and binding activities. *J Biol Chem.* 2004 Dec 17;279(51):53691–8.
 43. Liriano MA, Varney KM, Wright NT, Hoffman CL, Toth EA, Ishima R, et al. Target binding to S100B reduces dynamic properties and increases Ca(2+)-binding affinity for wild type and EF-hand mutant proteins. *J Mol Biol.* 2012 Oct 26;423(3):365–85.
 44. Masuda T, Kigo S, Mitsumoto M, Ohta K, Suzuki M, Mikami B, et al. Positive Charges on the Surface of Thaumatin Are Crucial for the Multi-Point Interaction with the Sweet Receptor. *Front Mol Biosci.* 2018 Feb 13;5:10.
 45. Prasad BVLS, Suguna K. Effect of pH on the structure of rhizopuspepsin. *Acta Crystallogr Sect D, Biol Crystallogr.* 2003 Oct;59(Pt 10):1755–61.
 46. Tang H, Shi K, Shi C, Aihara H, Zhang J, Du G. Enhancing subtilisin thermostability through a modified normalized B-factor analysis and loop-grafting strategy. *J Biol Chem.* 2019 Nov 29;294(48):18398–407.
 47. Knapp B, Deane CM. T-Cell Receptor Binding Affects the Dynamics of the Peptide/MHC-I Complex. *J Chem Inf Model.* 2016 Jan 25;56(1):46–53.

48. Pierce BG, Weng Z. A flexible docking approach for prediction of T cell receptor-peptide-MHC complexes. *Protein Sci.* 2013 Jan;22(1):35–46.
49. Armstrong KM, Piepenbrink KH, Baker BM. Conformational changes and flexibility in T-cell receptor recognition of peptide-MHC complexes. *Biochem J.* 2008 Oct 15;415(2):183–96.
50. Meeks SL, Healey JF, Barrow RT, Parker ET, Lollar P. Enhanced Anticoagulant Activity of Factor VIII Inhibitors Due to Positive Cooperativity between Two Classes of Anti-Factor VIII C2 Antibodies. *Blood.* 2007 Nov 16;110(11):784–784.
51. Walter JD, Werther RA, Polozova MS, Pohlman J, Healey JF, Meeks SL, et al. Characterization and solution structure of the factor VIII C2 domain in a ternary complex with classical and non-classical inhibitor antibodies. *J Biol Chem.* 2013 Apr 5;288(14):9905–14.
52. Burnett DL, Schofield P, Langley DB, Jackson J, Bourne K, Wilson E, et al. Conformational diversity facilitates antibody mutation trajectories and discrimination between foreign and self-antigens. *Proc Natl Acad Sci USA.* 2020 Sep 8;117(36):22341–50.
53. Moraes AH, Simonelli L, Pedotti M, Almeida FCL, Varani L, Valente AP. Antibody binding modulates conformational exchange in domain III of dengue virus E protein. *J Virol.* 2016 Feb 15;90(4):1802–11.

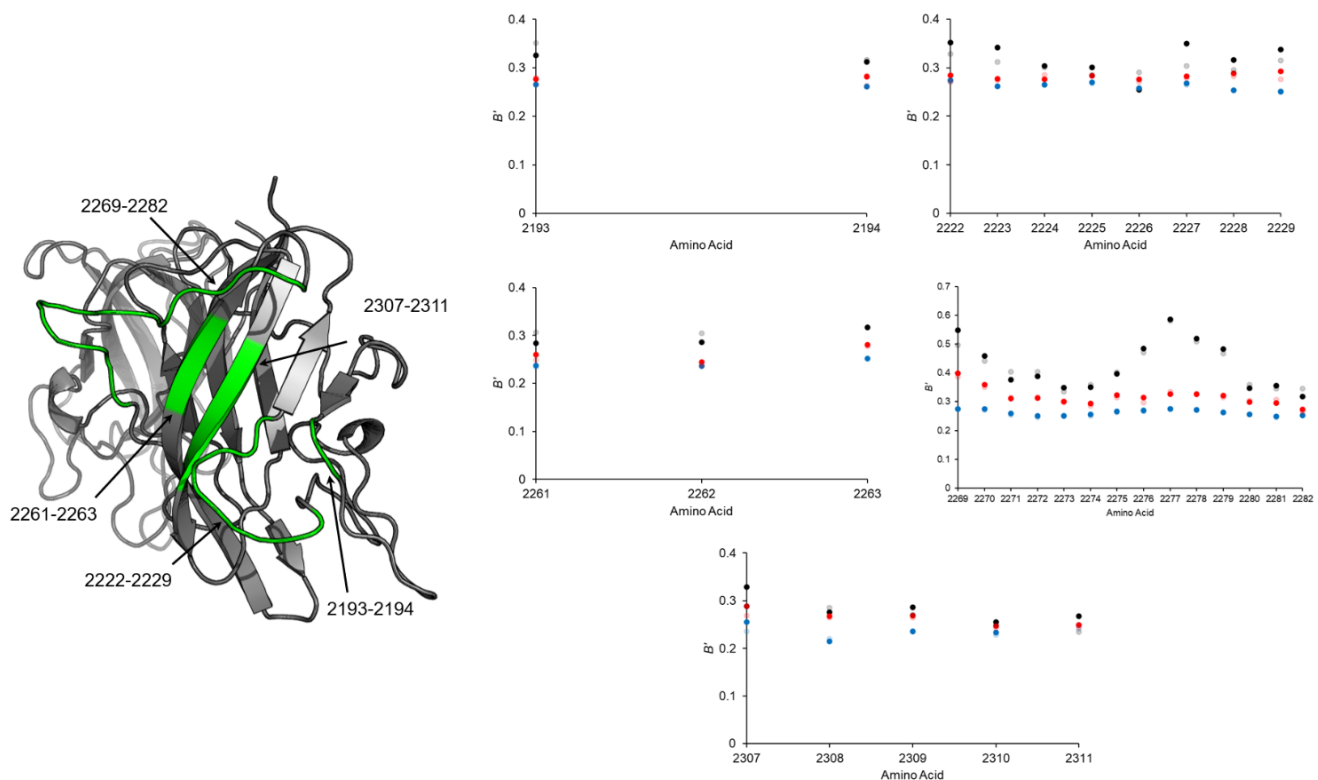
Supplementary Material

Table S1. X-ray data collection and refinement statistics.

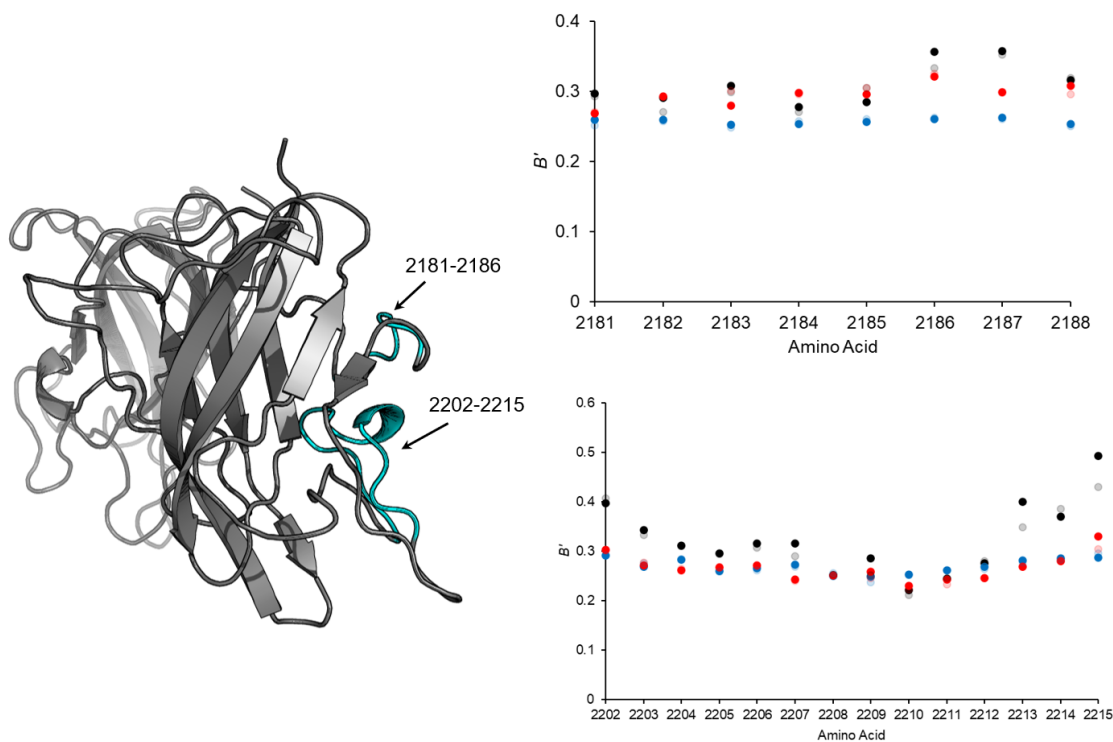
Wavelength (Å)	1
Resolution range (Å)	25.48 - 4.15 (4.298 - 4.15)
Space group	P 4 ₁ 2 ₁ 2
Unit cell	a = 132.243, b = 132.243, c = 380.029; α , β , γ = 90°
Total reflections	52,566 (50,92)
Unique reflections	26,284 (2,546)
Multiplicity	2.0 (2.0)
Completeness (%)	99.08 (98.31)
Mean I/sigma(I)	6.31 (0.48)
Wilson B-factor	195.91
R_{merge}	0.06373 (1.359)
R_{meas}	0.09012 (1.922)
R_{pim}	0.06373 (1.359)
CC1/2	0.998 (0.373)
CC*	1 (0.737)
Reflections used in refinement	26,198 (2,504)
Reflections used for R_{free}	1,987 (191)
R_{work}	0.2998 (0.4645)
R_{free}	0.3384 (0.4481)
Number of non-hydrogen atoms	11,366
macromolecules	11,293
ligands	73
Protein residues	1,444
RMS (bonds)	0.005
RMS (angles)	1.07
Ramachandran favored (%)	78.02
Ramachandran allowed (%)	15.15
Ramachandran outliers (%)	6.83
Rotamer outliers (%)	0.08
Clashscore	15.7
Average B-factor	253.38
macromolecules	253.25
ligands	273.82



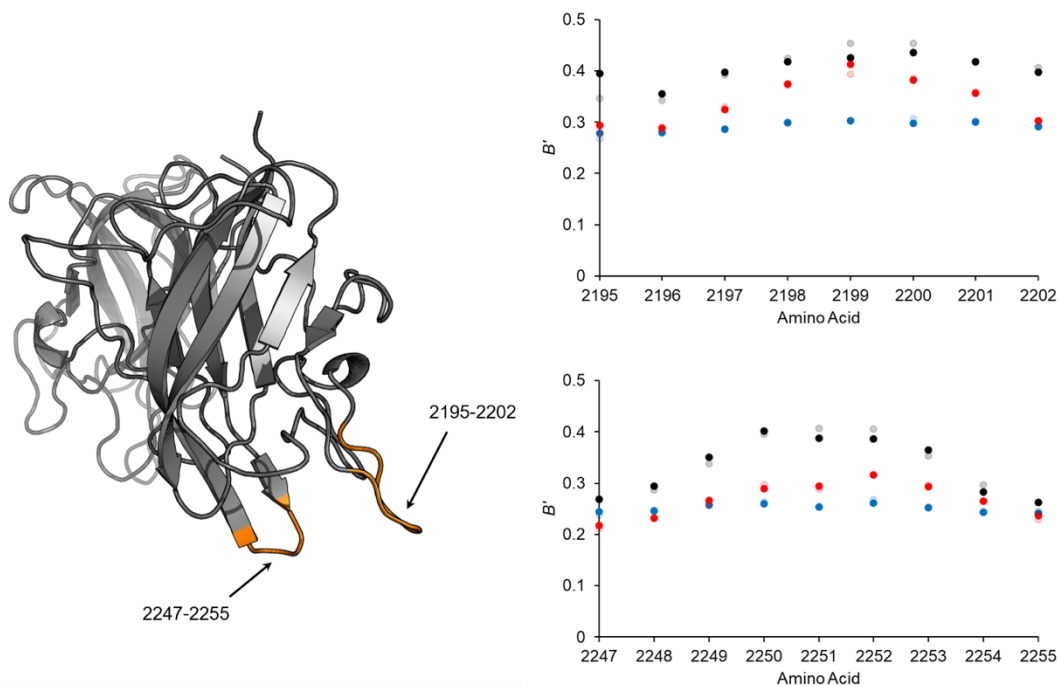
Supplementary Figure 1. Atomic B' values per amino acid for 2A9 epitope. (Left) Cartoon structure of the C1 domain highlighting 2A9 epitope (magenta). (Right) Solid circles represent the average B' of the amino acids and faded circles represent the B' value of the $C\alpha$ atoms from unbound ET3i (black, PDB ID: 6MF0), ET3i:G99 (blue, PDB ID: 7KBT), and ET3i:2A9 (red, PDB ID: 7K66).



Supplementary Figure 2. Atomic B' values per amino acid for G99 epitope. (Left) Cartoon structure of the C2 domain highlighting G99 epitope (green). (Right) Solid circles represent the average B' of the amino acids and faded circles represent the B' value of the $C\alpha$ atoms from unbound ET3i (black, PDB ID: 6MF0), ET3i:G99 (blue, PDB ID: 7KBT), and ET3i:2A9 (red, PDB ID: 7K66).



Supplementary Figure 3. Atomic B' values per amino acid for 3E6 epitope. (Left) Cartoon structure of the C2 domain highlighting 3E6 epitope (cyan). (Right) Solid circles represent the average B' of the amino acids and faded circles represent the B' value of the $C\alpha$ atoms from unbound ET3i (black, PDB ID: 6MF0), ET3i:G99 (blue, PDB ID: 7KBT), and ET3i:2A9 (red, PDB ID: 7K66).



Supplementary Figure 4. Atomic B' values per amino acid for BO2C11 epitope. (Left) Cartoon structure of the C2 domain highlighting BO2C11 epitope (orange). (Right) Solid circles represent the average B' of the amino acids and faded circles represent the B' value of the $C\alpha$ atoms from unbound ET3i (black, PDB ID: 6MF0), ET3i:G99 (blue, PDB ID: 7KBT), and ET3i:2A9 (red, PDB ID: 7K66).